Regional advanced very high resolution radiometer–derived climatology of aerosol optical thickness and size

Igor V. Geogdzhayev,[1] Michael I. Mishchenko,[2] Edward I. Terez,[3] Galina A. Terez,[4] and Genady K. Gushchin[5]

Received 25 April 2005; revised 2 August 2005; accepted 26 September 2005; published 3 December 2005.

[1] We have used the NASA Global Energy and Water Cycle Experiment (GEWEX) Global Aerosol Climatology Project data set of retrieved aerosol optical thickness and Ångström exponent to construct and analyze regional aerosol climatologies for a number of areas affected by different aerosol types (such as dust, biomass burning, anthropogenic, or clear maritime aerosols) that exemplify the range of natural aerosol variation. We have found that variations in the number of individual pixels used to calculate monthly means associated with short- and long-term satellite orbit changes and instrument degradation have little effect on global and hemispherical values of the aerosol optical thickness and Ångström exponent. Aerosol loads are found to be higher, and aerosol particles smaller, over the northern Atlantic Ocean off the coast of Europe and the eastern United States, rather than off the west coast, thereby indicating a significant impact of anthropogenic aerosols. The smallest background levels of maritime aerosols are found in the southern Pacific Ocean, with seasonal mean optical thicknesses as low as 0.1. We analyze time series of the aerosol optical thickness in the regions affected by dust outflows from the Sahara and Asian deserts and by biomass burning. An influence of anthropogenic aerosols associated with the high regional industrial activity is apparent in the eastern China Sea. Two distinct periods are identified in satellite and Sun photometer aerosol time series over the Black Sea with transition time around 1993. During the first period the aerosol loads in the region significantly exceeded the hemispherical mean, whereas in the second period they became very close. This change is linked to the reduction of the industrial output in that region.

Citation: Geogdzhayev, I. V., M. I. Mishchenko, E. I. Terez, G. A. Terez, and G. K. Gushchin (2005), Regional advanced very high resolution radiometer–derived climatology of aerosol optical thickness and size, *J. Geophys. Res.*, *110*, D23205, doi:10.1029/2005JD006170.

1. Introduction

[2] The aerosol effect on climate is currently the subject of intense scientific research. While for the estimation of the direct radiative forcing by various aerosol types the knowledge of their optical properties is sufficient, the quantification of the indirect effects through cloud-aerosol interactions will require a better understanding of the complex physical and chemical processes involved [*Hansen et al.*, 1998, 2002]. Furthermore, both tasks necessitate the knowledge of the global distribution of aerosol amount and type [*Mishchenko et al.*, 2004]. Because of their global coverage, satellite measurements are a unique instrument to obtain this knowledge.

[3] Recent years have been marked by the launch of several advanced satellite instruments, such as the Moderate resolution Imaging Spectrometer (MODIS), the Multiangle Imaging Spectroradiometer (MISR), and the Polarization and Directionality of the Earth's Reflectances (POLDER) sensor [*Tanré et al.*, 1997; *Kahn et al.*, 2001; *Goloub et al.*, 1999]. One of the stated objectives of these instruments is to retrieve aerosol properties on a global scale. Other missions are being planned and developed [*Mishchenko et al.*, 2004].

[4] Another important recent activity has been to reprocess the data from the older instruments which, albeit not specifically designed for aerosol research, can yield valuable long-term records of aerosol properties unavailable with the newer instruments [*Nakajima and Higurashi*, 1998; *Torres et al.*, 1998; *Mishchenko et al.*, 1999; *Ignatov and Stowe*, 2002; *Ignatov et al.*, 2004; *Chiapello and Moulin*, 2002]. A global climatology of the aerosol optical thickness and Ångström exponent developed in the framework of the Global Aerosol Climatology Project (GACP) [*Mishchenko et al.*, 2002] is derived from channel 1 and 2 radiances of the advanced very high resolution radiometer (AVHRR) instruments on board of NOAA-7, -9, -11, and -14 platforms. It now covers the period from July 1983

[1]Columbia University, NASA Goddard Institute for Space Studies, New York, New York, USA.
[2]NASA Goddard Institute for Space Studies, New York, New York, USA.
[3]Crimean Astrophysical Observatory, Simferopol, Ukraine.
[4]National Taurida Vernadsky University, Simferopol, Ukraine.
[5]Karadag Research Geophysical Observatory, Feodosia, Ukraine.

0148-0227/05/2005JD006170$09.00

through September 2001 and, hopefully, will soon be further extended once the data from the NOAA-16 AVHRR have been processed. Since the beginning of the project in 1998, the retrievals have been compared with ground-based, airborne, and modeling data [*Kinne et al.*, 2001; *Haywood et al.*, 2001; *Penner et al.*, 2002; *Mishchenko et al.*, 2003; *Yu et al.*, 2003; *Myhre et al.*, 2004; *Jeong et al.*, 2005]. Recently, *Liu et al.* [2004] have shown that the retrieval results are in good agreement with an extensive set of shipborne Sun photometer data. As a result of these comparisons several modifications to the retrieval algorithm have been made over the years that, we believe, have improved the overall accuracy of the final product. The latest version of the product is available on the World Wide Web at http://gacp.giss.nasa.gov/retrievals.

[5] *Mishchenko et al.* [2003] analyzed time series of the retrieved aerosol optical depth and Ångström exponent for several large regions using an earlier version of the GACP product. In this paper, we use the latest version of the retrieval algorithm and the extended data record to analyze a representative set of time series for regions affected predominantly by specific aerosol types.

[6] As discussed by *Mishchenko et al.* [1999], the accuracy of GACP retrievals is limited by the calibration uncertainties, which makes it difficult to anticipate the detection of weak trends in the global aerosol load as needed for climate studies. However, one may still be able to detect long-term regional changes exceeding those in the globally averaged aerosol record.

[7] The GACP retrieval algorithm is based on the following modified power law aerosol size distribution [*Mishchenko et al.*, 1999]:

$$n(r) = \begin{cases} C, & r \le r_1, \\ C\left(\dfrac{r}{r_1}\right)^{-\alpha}, & r_1 < r \le r_2, \\ 0, & r > r_2 \end{cases} \tag{1}$$

with $r_1 = 0.1$ μm, $r_2 = 10$ μm, and $\alpha \in [2.5, 5]$. The normalization constant C is chosen such that

$$\int_0^\infty \mathrm{d}r\, n(r) = 1. \tag{2}$$

Aerosol particles are assumed to be perfect spheres with a wavelength-independent refractive index $m = 1.5 + 0.003i$. For a complete description of the assumption used in the algorithm we refer to *Mishchenko et al.* [1999] and *Geogdzhayev et al.* [2002, 2004].

[8] The availability of only two pieces of information per pixel (radiances in AVHRR channels 1 and 2) forces us to apply the above aerosol model globally and to fix the values of the parameters in equation (1) as well as the aerosol refractive index. Only the Ångström exponent (which is a unique function of α) is retrieved along with the aerosol optical thickness.

[9] This approach is chosen with the goal of minimizing long-term statistical errors of the global aerosol values retrieved by the algorithm. However, it leaves the possibility that regional retrievals can be biased in areas dominated by aerosol types significantly different from the model assumptions. For example, comparisons with MODIS and MISR data showed that while the general structure of the global aerosol field retrieved by all three instruments is remarkably similar, there are significant regional differences [*Geogdzhayev et al.*, 2004]. However, our present analysis refers mostly to the relative properties of the regional time series, which gives us confidence that the main conclusions reached will hold even if further changes in the algorithm are found to be desirable in the future.

2. Influence of Satellite Orbit Drift on Global Aerosol Means

[10] Owing to the specific character of the Sun-synchronous orbit of the NOAA satellites, aerosol retrievals are only possible within a seasonably variable latitudinal belt. In addition to the seasonal variation, the belt boundaries change over time as the satellite orbit drifts. These effects are illustrated in Figure 1, which shows the time series of the global monthly mean aerosol optical thickness (top) and the number of individual pixels that have gone into the calculation of the means (bottom). The most pronounced features of the optical thickness time series are the seasonal variability of the global and hemispherical means and the blueprints of the two major volcanic eruptions: El Chichon (March 1982) and Pinatubo (June 1991) (see *Geogdzhayev et al.* [2004] and *Mishchenko et al.* [2003] for further discussions of the GACP data set). Four distinct time periods are easily identified in the bottom plot, which corresponds to the four different NOAA platforms. One can see that within each period, the number of pixels progressively diminishes as the orbital drift makes more frequent the occurrence of low-illumination conditions unsuitable for aerosol retrievals. The sharp decreases in the number of points at the end of operation of the NOAA-11 and -14 platforms in 1994 and 2001, respectively, are associated with general instrument failures and the corresponding data quality deterioration.

[11] It is important to note that the dramatic changes in the usable-pixel statistics within a satellite lifetime as well as at times of transition from one instrument to another did not cause any discernable artifacts in the global aerosol record. We attribute this fact to the robustness of the retrieval algorithm.

[12] Smaller high-frequency changes in the number of pixels are associated with seasonal shifts of the latitudinal belt toward the poles. Because a greater fraction of the Northern Hemisphere is covered with land compared with the Southern Hemisphere, the shifts reduce or increase the number of pixels available for GACP aerosol retrievals over the ocean.

[13] To check if any artificial seasonality is present in the global and hemispherical GACP records, we plotted in Figure 2 the global and hemispherical seasonal means of aerosol optical thickness and Ångström exponent (solid curves) as well as corresponding variables in 30°S–30°N, 30°S–0°, and 0°–30°N latitudinal belts. One can see that the global and the 30°S–30°N means are very close throughout the data record, whereas during the periods free from the influence of volcanic eruptions the "belt" means exhibit slightly less variability compared to the corresponding hemispherical variables. This effect is more pronounced in the Southern Hemisphere due to the exclu-

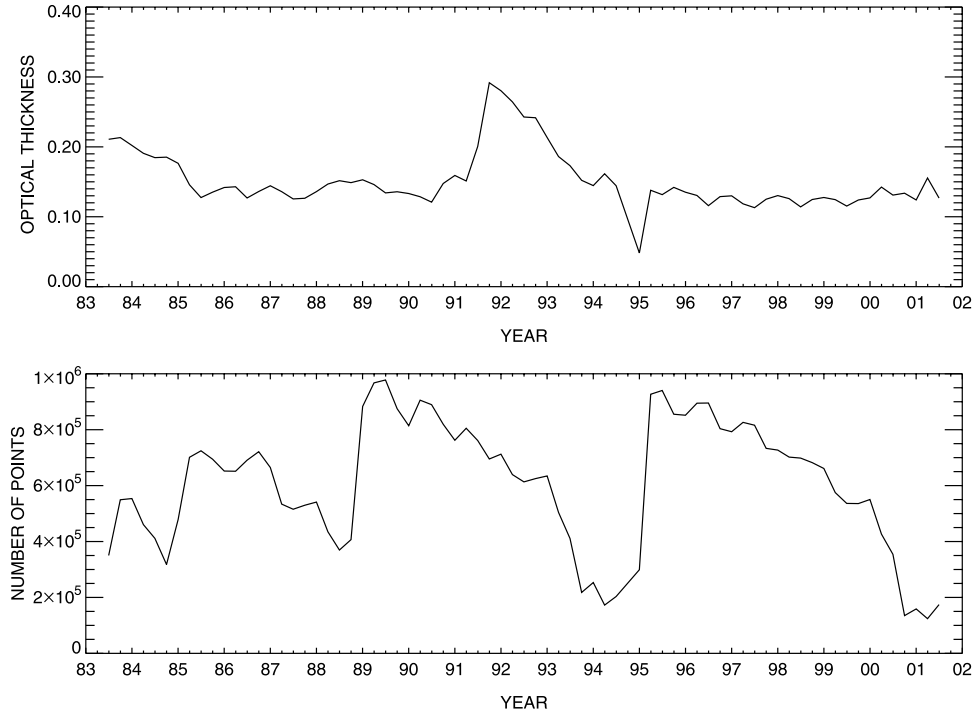

Figure 1. (top) Time series of the global monthly mean aerosol optical thickness and (bottom) the number of individual pixels used to compute the mean.

sion of the higher-aerosol-load middle latitudes (usually associated with increased sea-salt loads) from the "belt" means. For the same reason the southern "belt" aerosol optical thickness also tends to be lower, by 0.01 to 0.02, than the full hemispherical mean.

[14] The Ångström exponent records exhibit similar behavior, with the global and the corresponding "belt" values being very close and the hemispherical "belt" means showing slightly less variability compared with the full hemispherical means. In addition in the Northern Hemi-

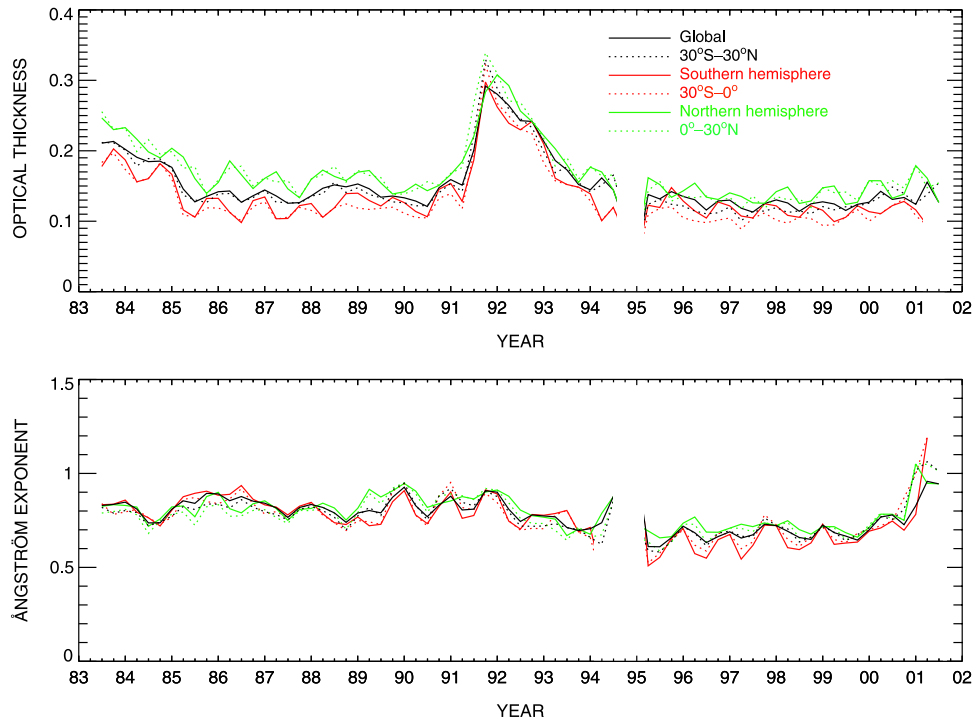

Figure 2. (top) Time series of the global and hemispherical seasonal mean values of the aerosol optical thickness (solid curves) and (bottom) Ångström exponent (solid curves). Also shown are seasonal values in the 30°S–30°N, 30°S–0°, and 0°–30°N latitudinal belts (dashed curves).

Table 1. Geographic Boundaries of the Regions

Region Description	Coordinates of the Border				Mean		Figure Number
	West	East	North	South	AOT	Angström Exponent	
U.S. east coast	82°W	70°W	45°N	25°N	0.152	0.88	4
	70°W	60°W	45°N	35°N			
U.S. west coast	130°W	115°W	45°N	25°N	0.13	0.74	4
Northern Atlantic off the coast of Europe	12°W	7.5°E	60°N	43°N	0.182	0.88	4
Northern Pacific Ocean	180°W	140°W	0°	40°N	0.134	0.78	5
Southern Pacific Ocean	170°W	110°W	0°	40°S	0.116	0.75	5
Southern Indian Ocean	60°E	100°E	10°S	40°S	0.122	0.74	5
Northern tropical Atlantic Ocean off the west coast of Africa	40°W	0°	35°N	5°N	0.218	0.73	6
Persian Gulf and Red Sea	30°E	75°E	30°N	8°N	0.219	0.77	6
Atlantic Ocean off the South African west coast	0°	20°E	0°N	25°S	0.22	0.79	6
Area off the Pacific coast of South America	80°W	70°W	5°N	30°S	0.194	0.76	6
	90°W	80°W	5°N	15°S			
Bay of Bengal	80°E	95°E	23°N	6°N	0.2	0.82	7
South China Sea	110°E	120°E	20°N	10°N	0.184	0.8	7
	110°E	114°E	10°N	6°N			
East China Sea	115°E	128°E	25°N	40°N	0.266	0.923	7
Sea of Japan	128°E	141°E	50°N	35°N	0.19	0.89	7
Eastern Black Sea	34°E	43°E	44°N	40°N	0.185	0.94	8
Western Black Sea	27°E	34°E	47°N	42°N	0.215	0.97	8
Eastern Mediterranean Sea	15°E	36°E	37°N	30°N	0.162	0.87	8

sphere the ''belt'' Ångström exponent means are almost always smaller that the corresponding full values, thereby indicating a reduced influence of smaller anthropogenic particles.

[15] We can, therefore, conclude that the effects of the variable pixel number and seasonal shifts of the latitudinal belt where the retrievals are possible on the global and hemispherical mean aerosol optical thickness are small and, if present, are less than the natural range of seasonal and zonal variation. Low correlation coefficients between the aerosol optical thickness and Ångström exponent and the number of pixels used to calculate these values (less than 0.08 absolute value for the global and hemispherical optical thicknesses and less than 0.28 for the Ångström exponent) further corroborate this statement. For regional time series considered below the corresponding correlation coefficients are also low: less than 0.34 for the optical thickness and 0.47 for the Ångström exponent. These conclusions agree well with the analysis of *Geogdzhayev et al.* [2004], who showed that the retrieved aerosol optical thickness compares well with contemporaneous data from MODIS and MISR. The latter instruments have a larger coverage and should, therefore, be less affected by these effects.

[16] Differences in the equator crossing times and the significant orbital drift of the NOAA satellites can potentially introduce a bias due to the aerosol diurnal cycle. However, the absence of any visible satellite-specific trends in the time series allows us to believe that the effect of aerosol diurnal cycle on the retrieval results is small.

3. Regional Time Series of Aerosol Optical Thickness and Ångström Exponent

[17] In this and the following sections, we will discuss time series of seasonal mean values of the aerosol optical thickness and Ångström exponent in various regions. The regions were selected to examine the influence of various aerosol types such as dust, biomass burning, and anthropogenic or clear maritime and to represent the range of natural aerosol variation. We chose to use seasonal rather than monthly means to accentuate the main features of the time series which otherwise may be obscured by the natural variation of aerosol properties. While the formal statistical errors of the data are quite small (the standard error of the regional seasonal mean is on the order of 0.01 or less for the optical thickness and 0.05 or less for the Ångström exponent), we do not believe that they reflect the true range of uncertainty associated with the retrievals as the main errors are likely to come from the uncertainty in calibration and the choice of globally fixed aerosol model parameters used in the retrieval algorithm. We refer the reader to *Mishchenko et al.* [1999] and *Geogdzhayev et al.* [2002] for an extensive sensitivity study which provides an estimate of these errors.

[18] Table 1 lists the exact geographic coordinates of the areas considered and gives the mean aerosol optical thickness and Ångström exponent for the periods not affected by major volcanic eruptions (this includes all measurements except those preceding July 1985 and those taken between June 1991 and December 1994). Figure 3 shows the corresponding borders overlaid on the map of monthly mean aerosol optical thickness for July 1986.

[19] Figure 4 shows the time series of the aerosol optical thickness and Ångström exponent for the areas off the west and east coast of the United States and the northern Atlantic Ocean off the coast of Europe. We did not include into consideration the area off the coast of Portugal and western Mediterranean Sea because they may be influenced by the dust outflows from Africa. The three curves have similar temporal dependence. The highest aerosol load is observed off the European coast followed by the U.S. east coast, while the cleanest air is found off the U.S. west coast. The observed differences are quite significant and can be as high as 0.1 for Europe and the U.S. west coast and 0.05 between the east and west coasts. An examination of the corresponding Ångström exponent plot reveals that the aerosol particles over Europe and the U.S. east coast are consistently smaller (Ångström exponents higher by about 0.2) than off the west coast. This can be explained by the larger fraction of smaller anthropogenic particles over Europe and the U.S. east coast and/or by the possible presence of desert dust originating from North American deserts in the outflow over the Pacific Ocean. These features

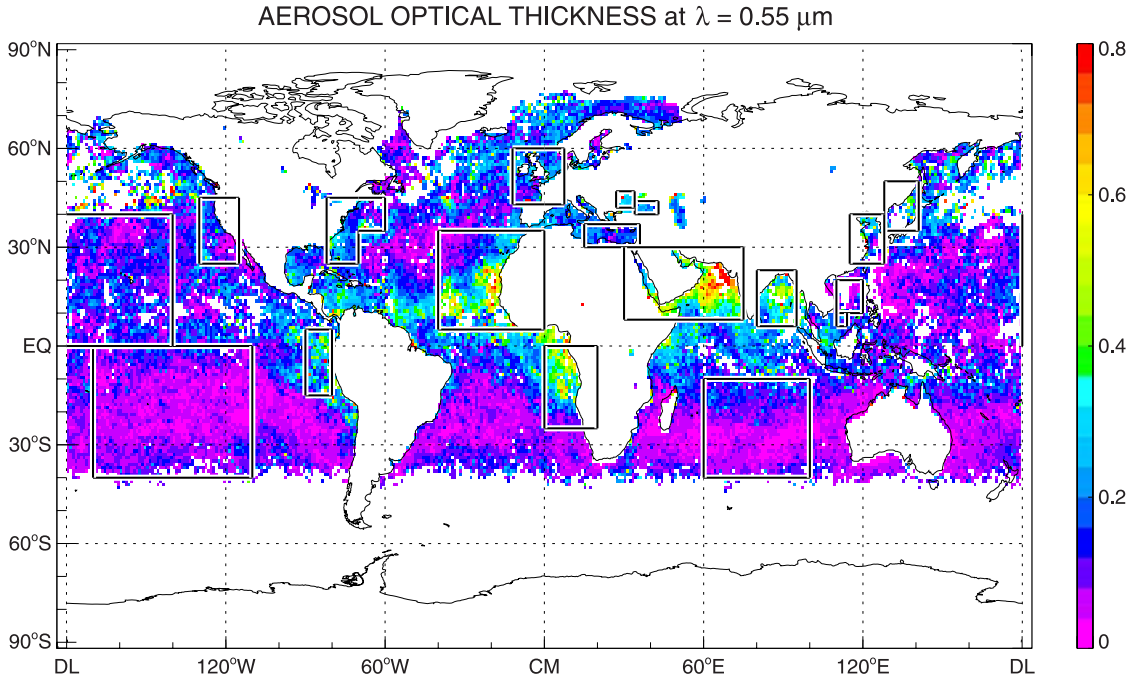

Figure 3. Geographical boundaries of the regions listed in Table 1 superposed on the color map of the monthly mean aerosol optical thickness for July 1986.

are in good agreement with ground-based aerosol observations [*Holben et al.*, 2001].

[20] Figure 5 illustrates the background levels of maritime aerosols found in the southern and northern Pacific Ocean and in the southern Indian Ocean. The specific regions' boundaries were chosen to avoid the major influences of aerosol outflows from the continents. The southern Pacific is one of the cleanest regions having the aerosol optical thickness fluctuating around 0.1 during volcano-free periods. Seasonal increases of the aerosol load during summer seasons in the Southern Hemisphere, especially noticeable in the eighties and (to a lesser extent) in the late nineties, are

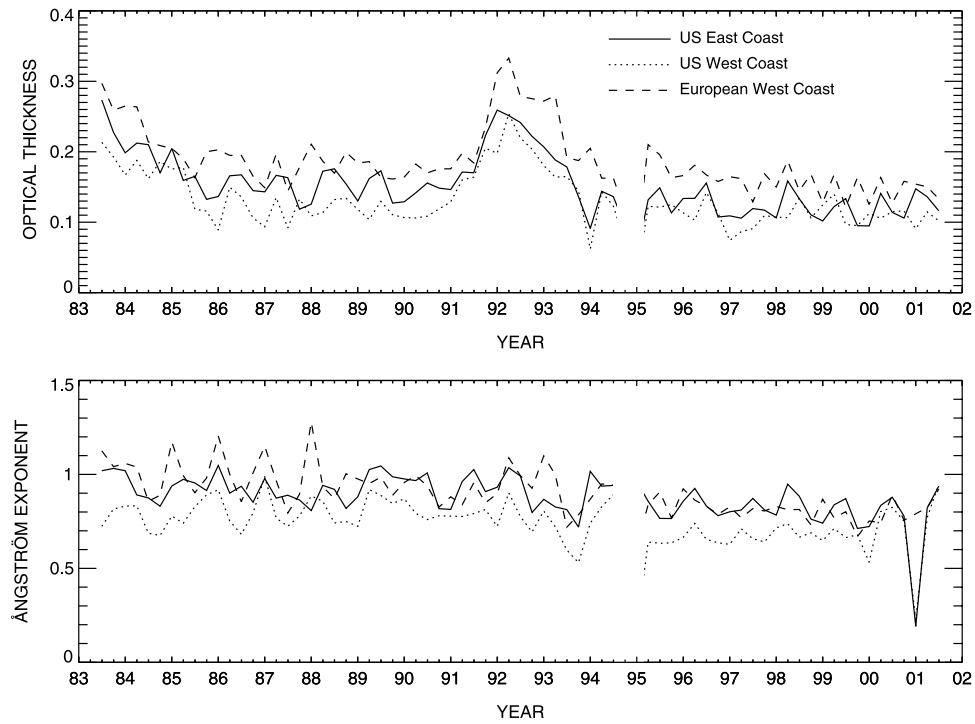

Figure 4. (top) Time series of seasonal mean values of the aerosol optical thickness and (bottom) Ångström exponent for the northern Atlantic Ocean off the U.S. east coast and off the coast of Europe, as well as for the area off the U.S. west coast.

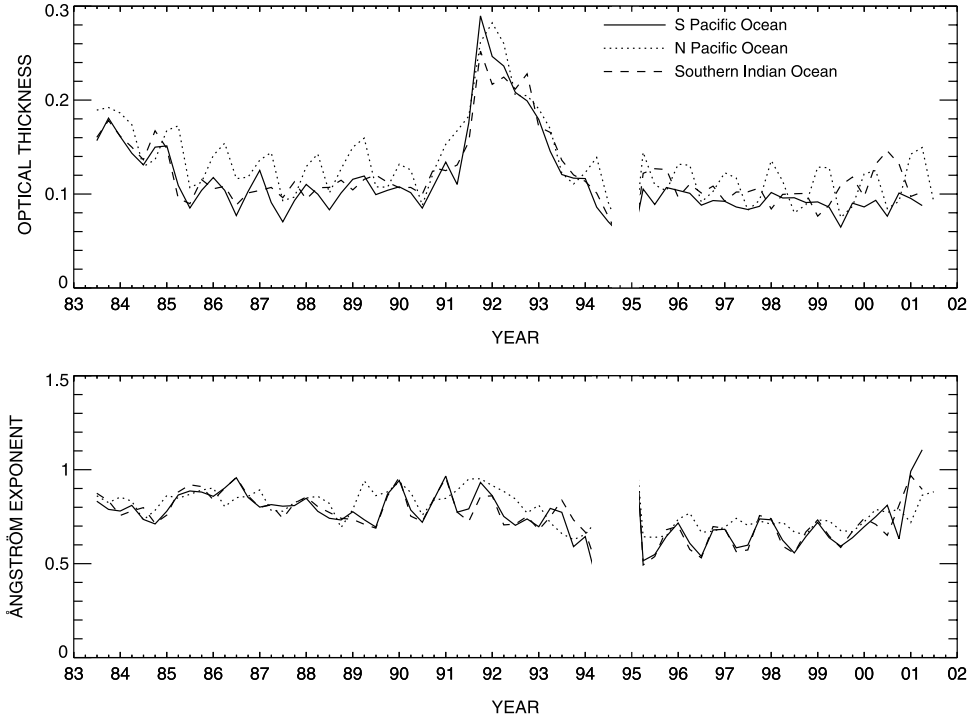

Figure 5. Same as in Figure 4, but for the southern and northern Pacific Ocean and the southern Indian Ocean.

probably associated with fires in the southeastern Asia and South America (note that since the background aerosol levels are low, even relatively small events can significantly influence the average).

[21] The northern Pacific has a somewhat higher aerosol load with a mean of 0.12 and slightly smaller particles (higher Ångström exponent values) compared with the coarser background maritime aerosols dominating the southern Pacific Ocean. This may indicate an anthropogenic influence. The seasonal changes of background aerosol loads in the northern Pacific with maxima occurring in spring may be a signature of the Asian dust events. The southern Indian Ocean's aerosol optical thickness record is close to but slightly higher than that in the southern Pacific, probably because of some residual dust contamination. The Ångström exponent is very close to that in the southern Pacific and, as expected in case of the presence of the coarser dust fraction, is lower than in the northern Pacific.

[22] Figure 6 shows the time series for regions affected by dust and/or biomass burning: northern tropical Atlantic Ocean off the west coast of Africa, the Persian Gulf and the Red Sea, the area off the South African west coast, and the area off the Pacific coast of South America. While the main feature in the first two regions is seasonal outflows of the desert dust from the continents the other two regularly experience major biomass burning events. One should keep in mind that dust and biomass burning aerosol outflows over the ocean occur at varying locations and times due to changes in the sources and wind patterns. Therefore the quantitative results depend on the choice of the geographic boundaries of a region.

[23] Because of the compactness of the Persian Gulf area and the regularity and intensity of dust events, this is where the highest aerosol loads are found. In the northern tropical Atlantic Ocean the maxima are lower due to the mixing of clean maritime air. Because the Saharan dust events last longer the corresponding Atlantic Ocean record shows higher background aerosol levels and smoother peaks compared with the Gulf area. The presence of dust particles, which tend to be larger than the background aerosols, is most apparent in the Ångström exponent record for the Gulf area, again due to the higher concentration of dust-loaded pixels contributing to the seasonal average. A well-defined seasonal biomass-burning pattern of aerosol load maxima is apparent off the South African west coast. One may also notice that the Ångström exponent tends to be smaller (larger particles) in dust-dominated regions compared with the areas affected by biomass burning.

[24] Figure 7 shows plots for several areas in Asia, such as the Bay of Bengal, the South and East China Seas, and the Sea of Japan. All four regions are characterized by periods of high aerosol loads, but the timing of their occurrence and the particle size are significantly different. It is interesting to note that while the East China Sea has the highest aerosol loads of the four regions, it also has relatively small particles. This may be an indication of the influence of anthropogenic aerosols associated with industrial activity in the region. The Ångström exponent time series for the South China Sea and Bay of Bengal follow each other closely and show lower values compared to the Sea of Japan and East China Sea. The corresponding aerosol optical thickness series reveal that the maxima in the South China Sea often occur during the periods of minima in the Bay of Bengal. These facts may indicate that the two regions are affected by the outflow of dust particles of similar composition and, possibly, the same sources (Asian deserts), with the temporal patterns determined by the regional meteorological conditions.

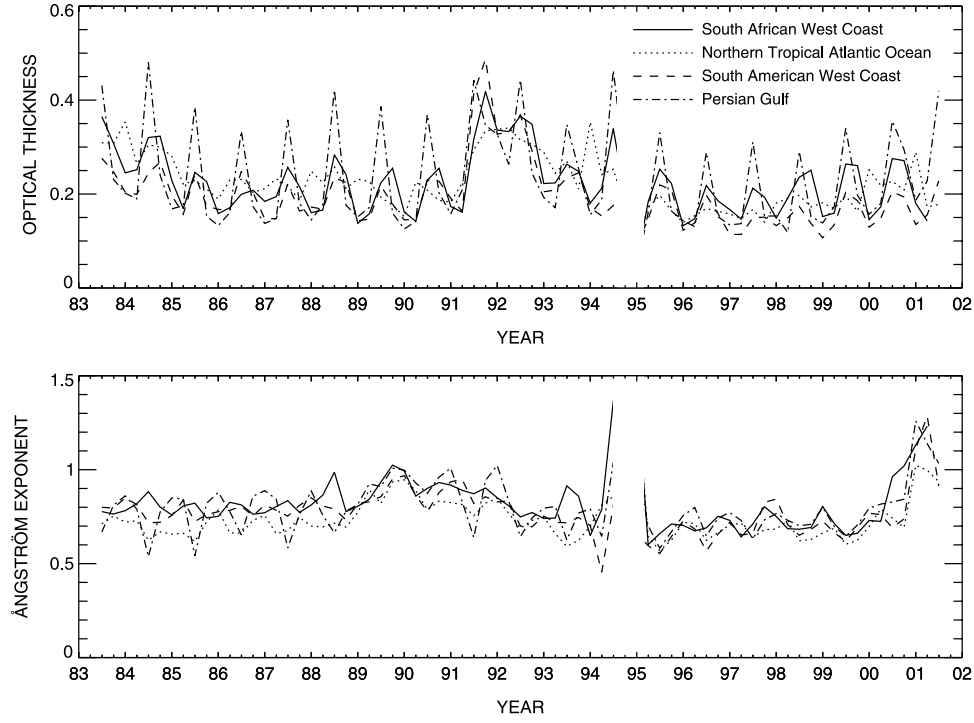

Figure 6. Same as in Figure 4, but for the northern tropical Atlantic Ocean off the west coast of Africa, the Persian Gulf and the Red Sea, the area off the South African west coast, and the area off the Pacific coast of South America.

[25] At the request of one of the reviewers of this paper we would like to suggest an explanation why the signature of the volcanic aerosols from the Mt. Pinatubo eruption is not apparent in neither regional nor global time series described above. As we discussed in *Geogdzhayev et al.* [2004], the accuracy of the Angstrom exponent retrieval from AVHRR data is limited due to the use of two broad closely spaced channels. (Because the two retrieved param-

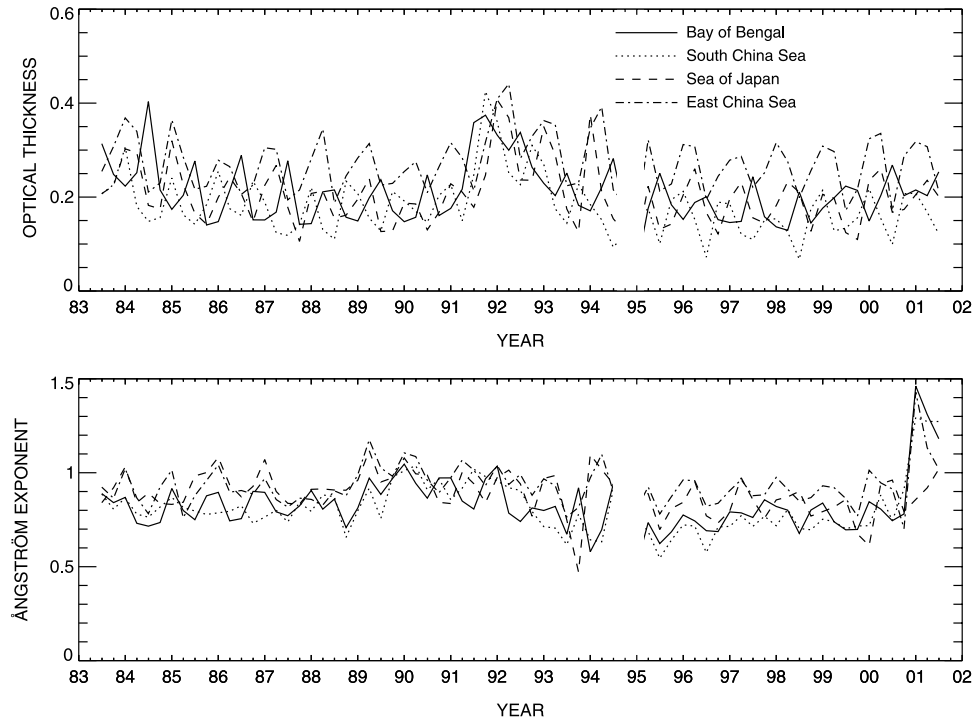

Figure 7. Same as in Figure 4, but for the Bay of Bengal, the South and East China Seas, and the Sea of Japan.

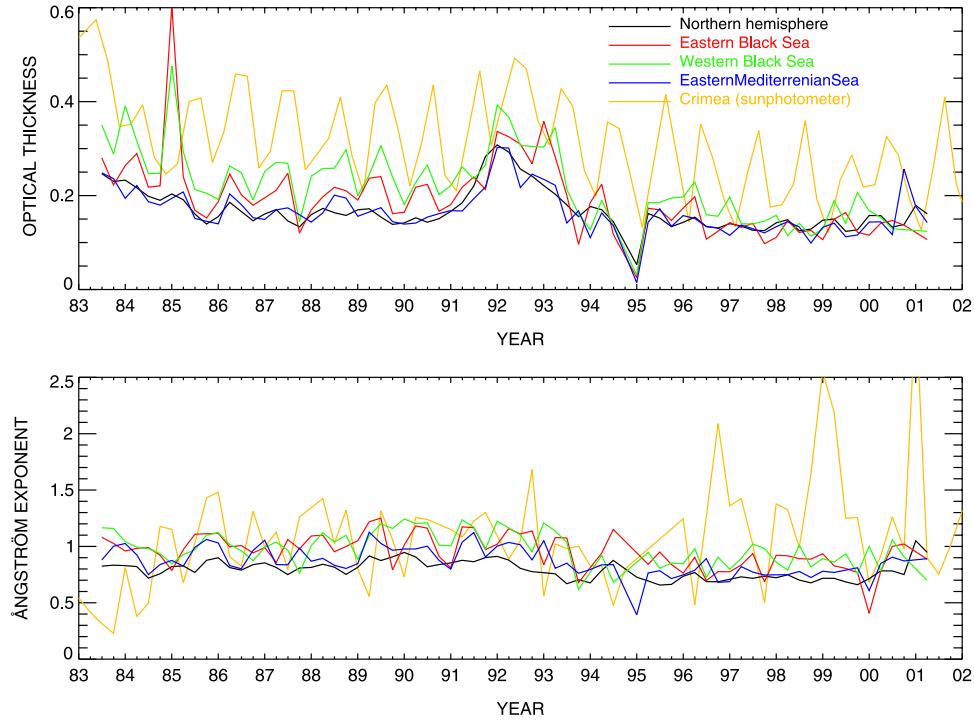

Figure 8. Same as in Figure 4, but for the western and eastern parts of the Black Sea and the eastern Mediterranean Sea. Also shown are the Northern Hemisphere seasonal means and the Sun photometer data in Crimea, Ukraine.

eters, optical thickness and Angstrom exponent, are largely orthogonal in the retrieval algorithm [*Geogdzhayev et al.*, 2004] we can refer independently to their accuracy.) Also, aerosol size distribution and optical properties assumed in the retrieval algorithm were chosen with the goal to minimize the long-term statistical errors in the global mean aerosol optical thickness and may not describe well volcanic aerosols. In addition, the volcanic aerosol was positioned above the most of the atmospheric water vapor and ozone, opposite to the assumptions in the atmospheric model in the retrieval algorithm. This may lead a spectral bias and therefore a systematic error in the retrieved Angstrom exponent. These limitations can make the detection of volcanic aerosol signature in the Angstrom exponent record difficult if not impossible. However, some of the features of the Angstrom exponent time series, such as seasonal cycles, higher values in dust-dominated regions and lower values in areas where anthropogenic influence is expected as well as global values close to those derived from MODIS make us believe that the Angstrom exponent record contains some useful information about the nature of the global aerosol distribution. At the same time it is worth noting that the Mt. Pinatubo volcanic aerosol signature is absent in the Sun photometer data in Crimea, Ukraine (see the next section) as well, providing (at least for that particular region) an independent validation of the satellite Angstrom exponent record.

4. Aerosol Changes Over the Black Sea

[26] In this section we discuss aerosol data record for the Black Sea region. There are two main reasons why a special section should be devoted to this topic. First, it is the only region where a significant change in aerosol amount could be identified in our data. Second, a contemporaneous long-term Sun photometer data set was available at a coastal site in the region, which independently confirms and helps to interpret the change in the satellite record.

[27] Figure 8 shows time series of the aerosol optical thickness and Ångström exponent for the eastern and western parts of the Black Sea and the eastern Mediterranean Sea. The records for the whole Northern Hemisphere are shown as a reference. Also shown in the figure are the aerosol optical thickness and Ångström exponent derived from the data obtained at an actinometric station located on the Crimean peninsula near Feodosia, Ukraine (44°54′N and 35°12′E). The measurements were made using an M-83 photometer in five spectral bands centered at 347, 368, 530, 574, and 638 nm. The instrument was located on the seashore at an elevation of 42 m. For an in-depth discussion of the full data set and the instrument the reader is referred to *Terez and Terez* [2002] and references therein.

[28] The data shown here is a part of the long-term measurement record covering the period from 1972 to the present. Seasonal averages of the aerosol optical thickness and Ångström exponent were calculated for comparison with the satellite data. The optical thickness was interpolated to 550 nm. The Ångström exponent values were calculated using the 369 nm and 638 nm channels.

[29] One can identify two distinct periods in the figure. During the first one, the aerosol loads over the Black Sea significantly exceeded the hemispherical mean. During the second period the two records become very close to each other. The exact transition time between the periods is obscured by the influence of the Mt. Pinatubo eruption and a gap in the data record between the NOAA-11 and -14

satellites at the end of 1994. One can, however, estimate it to have occurred around 1993. This provides a strong indication that the change is associated with a reduction in anthropogenic aerosol amounts due to the political changes in the Eastern Europe and in the former Soviet Union and the resulting dramatic reduction in the industrial output in that region. The records for the eastern part of the Mediterranean Sea do not show any long-term changes in the aerosol load, with optical thickness values being equally close to the hemispherical mean during both periods. This is consistent with the fact that the region is affected by the air masses from the Western Europe, which did not experience a reduction in the industrial output.

[30] Further evidence for the proposed explanation comes from the Ångström exponent records that also reveal two different periods with roughly the same transition time. During the first period the Ångström exponent over the Black Sea is significantly higher on average compared to the hemispherical mean than during the second period. The higher apparent Angström exponent values may be caused directly by the presence of smaller anthropogenic aerosol particles or, alternatively, may result from the change in the ocean color associated with industrial and shipping activities. It is not possible to separate the two causes from the satellite data alone. Because the observed changes are relative and do not happen at the time of transition from one satellite to another, one can exclude calibration problems as an alternative explanation.

[31] One can also notice that the observed reduction in the aerosol optical thickness is larger in the western part of the Black Sea (an average aerosol optical thickness difference between the two periods $\Delta\tau = 0.08$) compared to the eastern part ($\Delta\tau = 0.06$). Several big ports are located on the western coast of the sea and are connected by busy boat routes. This may have had a two-fold effect on the retrieved aerosol record. First, the reduction in the shipping associated with diminishing industrial output may have directly reduced the aerosol loads in the region. Second, it may have resulted in reduced sea pollution making the sea surface darker. This would have reduced the retrieved aerosol optical thickness. Again, it is not possible to separate the two effects using the AVHRR data alone.

[32] We compared the satellite data to the ground-based aerosol record from the Crimea peninsula. The Sun photometer data are characterized by large seasonal variations. While observed winter minima are close to the satellite record, the summer maxima are significantly higher, with optical depths as high as 0.4. This may indicate the influence of mineral aerosols from more arid areas further inland in the summer as well as local meteorological conditions specific to the coastal site.

[33] The two distinct periods with the same transition time are also apparent in the Sun photometer optical thickness data. The ground-based Ångström exponent record shows values consistent with the satellite data for most of the satellite record duration, with several periods of very large Ångström exponent values (up to 2.5). The exact reason for such high Ångström exponent values is not known. An examination of the full Sun photometer data set (beginning in 1972) shows that similarly large Ångström exponent values (exceeding 1.8) were observed in the late 1970s to the early 1980s. Additional research is needed to establish whether the observed variations of the Angström exponent reflect the range of its natural variability, weather pattern, or local changes at the site. One should also note that the current AVHRR aerosol retrieval algorithm does not allow the retrieval of Ångström exponent values higher that about 1.75. In addition, different screening procedures used in the satellite and ground-based algorithms may have contributed to the discrepancy. On one hand, the satellite retrievals utilize all pixels deemed to be cloud-free. On the other hand, the Sun photometer site is affected by frequent occurrences of thin cirrus clouds and haze in the winter; such days are typically excluded from the calculation of the Ångström exponent. Residual contamination of satellite measurements by clouds and/or sea foam would have the effect of reduced Ångström exponents.

[34] Increased atmospheric transparency in the region due to the reduced industrial output has been reported by *Terez and Terez* [2002]. This result can find applications in the climate forcing modeling. Specifically, it can provide a constraint for aerosol transport models for a major source area of man-made atmospheric aerosols.

[35] Given the scale of economic changes in the Eastern Europe and the former Soviet Union it is possible that the associated reduction in the industrial output (over 50%) has had larger-scale effects on aerosol loads. Long-term observations in Moscow, Russia and Tartu, Estonia [*Okulov*, 2003] show that atmospheric transparency increased in the nineties. In fact, as is indicated in [*Terez and Terez*, 2002; *Okulov*, 2003], by 1997 the aerosol load over the European part of the former Soviet Union has reached its preindustrial (before 1930) levels. Indications of the global effect of these changes are present in the AVHRR aerosol record as well: one can see (Figure 2) that for the periods not affected by volcano eruptions the gap between the mean aerosol optical thickness over the Northern (where the changes occurred) and Southern Hemispheres is bigger in the eighties compared to the nineties. A further test of this hypothesis will come from the planned extension of the satellite data record using the NOAA-16 data.

5. Conclusions

[36] We have used the GACP data set of the aerosol optical thickness and Ångström exponent to develop and investigate regional climatologies for a representative set of geographical areas affected by different aerosol types. Our analysis has led to the following conclusions.

[37] 1. Variations in the number of individual pixels used to calculate monthly means associated with short- and long-term satellite orbit changes and instrument degradation have little effect on the global and hemispherical values of the aerosol optical thickness and Ångström exponent.

[38] 2. Consistent with ground-based observations, aerosol loads are found to be higher and aerosol particles smaller over the northern Atlantic Ocean off the coast of Europe and off the U.S. east coast than off the U.S. west coast, thus potentially indicating a considerable influence of anthropogenic aerosols.

[39] 3. The smallest background levels of maritime aerosols are found in the southern Pacific Ocean with seasonal mean optical thicknesses as low as 0.1. Aerosol loads in the northern Pacific Ocean and in the southern Indian Ocean are

slightly higher, whereas the particles in the northern Pacific are smaller.

[40] 4. The highest seasonal values of the aerosol optical thickness are found in the Persian Gulf region during dust events. The area of the Atlantic Ocean affected by Saharan dust outflows shows higher background aerosol levels and smoother peaks.

[41] 5. Synchronized seasonal increases in the aerosol optical thickness are apparent in the time series for areas off the west coast of South Africa and South America.

[42] 6. The highest aerosol loads in Asia are found in the East China Sea where the particles also has relatively small sizes. This indicates the presence of anthropogenic aerosols associated with significant industrial activity in the region.

[43] 7. Two distinct periods are identified in the satellite and ground based (the Crimean peninsula) data in the Black Sea aerosol time series, with transition time around 1993. During the first period the aerosol loads in the region significantly exceeded the hemispherical mean, whereas during the second period the differences became much smaller. The change is linked to the reduction of anthropogenic aerosol amounts due to the political changes in the Eastern Europe and the former Soviet Union and the associated dramatic reduction in the industrial output in that region.

[44] **Acknowledgments.** We thank two anonymous reviewers for their comments that helped to improve the manuscript. This research was supported by the NASA Radiation Sciences Program, which is managed by Hal Maring.

References

Chiapello, I., and C. Moulin (2002), TOMS and METEOSAT satellite records of the variability of Saharan dust transport over the Atlantic during the last two decades (1979–1997), *Geophys. Res. Lett.*, *29*(8), 1176, doi:10.1029/2001GL013767.

Geogdzhayev, I. V., M. I. Mishchenko, W. B. Rossow, B. Cairns, and A. A. Lacis (2002), Global two-channel AVHRR retrievals of aerosol properties over the ocean for the period of NOAA-9 observations and preliminary retrievals using NOAA-7 and NOAA-11 data, *J. Atmos. Sci.*, *59*, 262–278.

Geogdzhayev, I. V., M. I. Mishchenko, L. Liu, and L. Remer (2004), Global two-channel AVHRR Aerosol climatology: Effects of stratospheric aerosols and preliminary comparisons with MODIS and MISR retrievals, *J. Quant. Spectrosc. Radiat. Transfer*, *88*, 47–59.

Goloub, P., D. Tanré, J. L. Deuzé, M. Herman, A. Marchand, and F. M. Bréon (1999), Validation of the first algorithm applied for deriving the aerosol properties over ocean using the POLDER/ADEOS measurements, *IEEE Trans. Geosci. Remote Sens.*, *37*, 1586–1596.

Hansen, J., M. Sato, A. Lacis, R. Ruedy, I. Tegen, and E. Matthews (1998), Perspective: Climate forcings in the industrial era, *Proc. Natl. Acad. Sci. USA*, *95*, 12,753–12,758.

Hansen, J., et al. (2002), Climate forcings in Goddard Institute for Space Studies SI2000 simulations, *J. Geophys. Res.*, *107*(D18), 4347, doi:10.1029/2001JD001143.

Haywood, J. M., P. N. Francis, I. Geogdzhayev, M. Mishchenko, and R. Frey (2001), Comparison of Saharan dust aerosol optical depths retrieved using aircraft mounted pyranometers and 2-channel AVHRR algorithms, *Geophys. Res. Lett.*, *28*, 2393–2396.

Holben, B. N., et al. (2001), An emerging ground-based aerosol climatology: Aerosol Optical Depth from AERONET, *J. Geophys. Res.*, *106*, 12,067–12,097.

Ignatov, A., and L. Stowe (2002), Aerosol retrievals from individual AVHRR channels. I. Retrieval algorithm and transition from Dave to 6S radiative transfer model, *J. Atmos. Sci.*, *59*, 313–334.

Ignatov, A., J. Sapper, S. Cox, I. Laszlo, N. Nalli, and K. Kidwell (2004), Operational aerosol observations (AEROBS) from AVHRR/3 on board NOAA-KLM Satellites, *J. Atmos. Oceanic Technol.*, *21*, 3–26.

Jeong, M., Z. Li, D. A. Chu, and S. Tsay (2005), Quality and compatibility analyses of global aerosol products derived from the advanced very high resolution radiometer and Moderate Resolution Imaging Spectroradiometer, *J. Geophys. Res.*, *110*, D10S09, doi:10.1029/2004JD004648.

Kahn, R., P. Banerjee, and D. McDonald (2001), Sensitivity of multi-angle imaging to natural mixtures of aerosols over ocean, *J. Geophys. Res.*, *106*, 18,219–18,238.

Kinne, S., et al. (2001), How well do aerosol retrievals from satellites and representation in global circulation models match ground-based AERONET aerosol statistics?, in *Remote Sensing and Climate Modeling: Synergies and Limitations*, edited by M. Beniston and M. M. Verstraete, pp. 103–158, Kluwer Acad., Norwell, Mass.

Liu, L., M. I. Mishchenko, I. V. Geogdzhayev, A. Smirnov, S. M. Sakerin, D. M. Kabanov, and O. A. Ershov (2004), Global validation of two-channel AVHRR aerosol optical thickness retrievals over the oceans, *J. Quant. Spectrosc. Radiat. Transfer*, *88*, 97–109.

Mishchenko, M. I., I. V. Geogdzhayev, B. Cairns, W. B. Rossow, and A. A. Lacis (1999), Aerosol retrievals over the ocean by use of channels 1 and 2 AVHRR data: Sensitivity analysis and preliminary results, *Appl. Opt.*, *38*, 7325–7341.

Mishchenko, M., J. Penner, and D. Anderson (Eds.) (2002), Global Aerosol Climatology Project, *J. Atmos. Sci.*, *59*, 249–783.

Mishchenko, M., I. V. Geogdzhayev, L. Liu, J. A. Ogren, A. A. Lacis, W. B. Rossow, J. W. Hovenier, H. Volten, and O. Muñoz (2003), Aerosol retrievals from AVHRR radiances: Effects of particle nonsphericity and absorption and an updated long-term global climatology of aerosol properties, *J. Quant. Spectrosc. Radiat. Transfer*, *79–80*, 953–972.

Mishchenko, M., B. Cairns, J. E. Hansen, L. D. Travis, R. Burg, Y. J. Kaufman, J. V. Martins, and E. P. Shettle (2004), Monitoring of aerosol forcing of climate from space: Analysis of measurement requirements, *J. Quant. Spectrosc. Radiat. Transfer*, *88*, 149–161.

Myhre, G., et al. (2004), Intercomparison of satellite retrieved aerosol optical depth over ocean, *J. Atmos. Sci.*, *61*, 499–513.

Nakajima, T., and A. Higurashi (1998), A use of two-channel radiances for an aerosol characterization from space, *Geophys. Res. Lett.*, *25*, 3815–3818.

Okulov, O. (2003), Variability of atmospheric transparency and precipitable water in Estonia during last decades, Ph.D. thesis, Inst. of Environ. Phys., University of Tartu, Tartu, Estonia.

Penner, J. E., et al. (2002), A comparison of model-and satellite-derived aerosol optical depth and reflectivity, *J. Atmos. Sci.*, *59*, 441–460.

Tanré, D., Y. J. Kaufman, M. Herman, and S. Mattoo (1997), Remote sensing of aerosol properties over oceans using the MODIS/EOS spectral radiances, *J. Geophys. Res.*, *102*, 16,971–16,988.

Terez, E. I., and G. A. Terez (2002), Investigation of atmospheric transmission in the Crimea (Ukraine) in the twentieth century, *J. Appl. Meteorol.*, *41*, 1060–1063.

Torres, O., P. K. Bhartia, J. R. Herman, and Z. Ahmad (1998), Derivation of aerosol properties from satellite measurements of backscattered ultraviolet radiation: Theoretical basis, *J. Geophys. Res.*, *103*, 17,099–17,110.

Yu, H., R. E. Dickinson, M. Chin, Y. J. Kaufman, B. N. Holben, I. V. Geogdzhayev, and M. I. Mishchenko (2003), Annual cycle of global distributions of aerosol optical depth from integration of MODIS retrievals and GOCART model simulations, *J. Geophys. Res.*, *108*(D3), 4128, doi:10.1029/2002JD002717.

I. V. Geogdzhayev, Columbia University, NASA Goddard Institute for Space Studies, 2880 Broadway, New York, NY 10025, USA. (igor@giss.nasa.gov)

G. K. Gushchin, Karadag Research Geophysical Observatory, Nauka Str., 10A, v. Kurortnoe, 98188, Feodosia, Ukraine.

M. I. Mishchenko, NASA Goddard Institute for Space Studies, 2880 Broadway, New York, NY 10025, USA.

E. I. Terez, Crimean Astrophysical Observatory, Box 1429, Simferopol, 95000, Ukraine.

G. A. Terez, National Taurida Vernadsky University, Box 1429, Simferopol, 95000, Ukraine.